ARMY RESEARCH LABORATORY

Strain Concentration Assessment of Laminates Subjected to Low Velocity Impact

Robert F. Anastasi and
Steven M. Serabian

ARL-TR-91 April 1993

The findings in this report are not to be construed as an official Department of the Army position unless so designated by other authorized documents.

Citation of manufacturer's or trade names does not constitute an official endorsement or approval of the use thereof.

Destroy this report when it is no longer needed. Do not return it to the originator.

REPORT DOCUMENTATION PAGE

Form Approved
OMB No. 0704-0188

1. AGENCY USE ONLY (Leave blank)	2. REPORT DATE	3. REPORT TYPE AND DATES COVERED
	April 1993	Final Report

4. TITLE AND SUBTITLE

Strain Concentration Assessment of Laminates Subjected To Low Velocity Impact

5. FUNDING NUMBERS

6. AUTHOR(S)

Robert F. Anastasi and Steven M. Serabian*

7. PERFORMING ORGANIZATION NAME(S) AND ADDRESS(ES)

U.S. Army Research Laboratory
Watertown, MA 02172-0001
ATTN: AMSRL-VS-V

8. PERFORMING ORGANIZATION REPORT NUMBER

ARL-TR-91

9. SPONSORING/MONITORING AGENCY NAME(S) AND ADDRESS(ES)

U.S. Army Research Laboratory
2800 Powder Mill Road
Adelphi, MD 20783-1145

10. SPONSORING/MONITORING AGENCY REPORT NUMBER

11. SUPPLEMENTARY NOTES

*Presently at ICAD, 201 Broadway Street, Cambridge, MA 02139-1901.

12a. DISTRIBUTION/AVAILABILITY STATEMENT

Approved for public release; distribution unlimited.

12b. DISTRIBUTION CODE

13. ABSTRACT (Maximum 200 words)

Low velocity impact upon composite laminates can lead to both apparent and nonapparent damage zones that result in structural strain concentrations. The strain concentrations can be, or grow to be, larger than permissible design levels through static or cyclic loading conditions thus drastically reducing the structural integrity of the composite component. In this paper, glass/epoxy composite coupons in three laminate orientations were damaged by low velocity impact that create a damage zone consisting of local fiber breakage and delamination. Conventional moire was then used to measure strain concentration as a function of applied tensile load. Correlations were made between impact energy, delamination area, strain concentration, and laminate orientation.

14. SUBJECT TERMS

Composite materials, Low velocity impact, Moire analysis, Strain analysis

15. NUMBER OF PAGES

19

16. PRICE CODE

17. SECURITY CLASSIFICATION OF REPORT	18. SECURITY CLASSIFICATION OF THIS PAGE	19. SECURITY CLASSIFICATION OF ABSTRACT	20. LIMITATION OF ABSTRACT
Unclassified	Unclassified	Unclassified	UL

Contents

Tables

Figures

Introduction

Increased performance requirements of both existing and future military hardware has necessitated increasing structural applications of composite materials. The attractiveness of these material systems is being compromised by their inherent damage susceptibility to low energy impact where the impactor does not penetrate the material but causes delamination through the thickness, as well as local fiber breakage. This damage causes structural degradation or reduced load carrying ability thus compromising structural integrity. A lack of knowledge bridging the gap between damage detection and structural integrity assessment has lead to highly conservative and costly repair procedures, as well as decreased "perceived" *lifetimes for specific composite* components. A correlation between low velocity impact parameters and resulting structural integrity in composite laminates is thus of prime importance.

In this paper, low velocity impact parameters of energy and visible damage zone size are correlated with resulting damage zone strain concentration factors. Conventional moire [1,2,3,4], full-field photomechanical displacement measurement technique, was used to obtain these strain concentration factors.

Experimental Measurements

Specimen Description

Impact test coupons, 1.5" x 7.0" were cut from the central sections of 3' x 3' laminated plates with a typical thickness of 0.125" that were manufactured from a 3M™ SP 250-S2 glass fiber/epoxy system. Three laminate orientations were manufactured $[(0/90)_4]_s$, $[(+45/-45)_4]_s$, and $[(0/+45/-45/90)_2]_s$. Ultimate tensile loads of the three laminates were obtained through the use of a streamline (SL-3) tension specimen design [5], as shown in Figure 1. The baseline ultimate tensile strengths for the corresponding orientations were 2250 lb, 600 lb, and 1900 lb for $[(0/90)_4]_s$, $[(+45/-45)_4]_s$, and $[(0/+45/-45/90)_2]_s$ orientations, respectively.

Figure 1. S-Glass streamline tensile coupon with a length of 6.0" and neck section width of 0.25".

Mechanical properties of the SP 250-S2 glass fiber/epoxy system obtained from manufacturer specification sheets are given in Table 1.

Table 1. Lamina mechanical properties

E_1	=	7.0E + 006 psi
E_2	=	2.1E + 006 psi
G_{12}	=	0.8E + 006 psi
υ_{12}	=	0.26

These values were used to find the effective two-dimensional laminate mechanical properties for the $[(0/90)_4]_S$, $[(+45/-45)_4]_S$, and $[(0/+45/-45/90)_2]_S$ laminate orientations using the classical laminate plate theory [6,7]. Results are given in Table 2.

Table 2. Effective in-plane laminate mechanical properties

Laminate	E'_x (psi)	E'_y (psi)	G'_{xy} (psi)	υ'_{xy}
$[(0/90)_4]_S$	4.64E + 006	4.64E + 006	0.8E + 006	0.12
$[(+45/-45)_4]_S$	1.70E + 006	1.70E + 006	1.02E + 006	0.53
$[(0/+45/-45/90)_2]_S$	1.34E + 006	1.34E + 006	0.47E + 006	0.29

These effective laminate mechanical values, along with the ultimate tensile strength values of the tensile tested SL-3 specimens, were used to calculate ultimate strength values for the impact test coupons. The impact test coupon ultimate strength values are 13,478 lb, 3594 lb, and 113,818 lb for the $[(0/90)_4]_S$, $[(+45/-45)_4]_S$, and $[(0/+45/-45/90)_2]_S$ laminate orientations, respectively.

Experimental Approach/Results

The experiment progressed in four stages: (1) impacting the coupons and measuring impact parameters, (2) measuring coupon damage areas, (3) applying moire, and (4) obtaining strain concentrations factors from displacement fringe contours.

The coupons were subjected to low velocity impact through the use of a 50-caliber light gas gun as is shown in Figure 2. The gas gun was fitted with a plastic sabot that carried a spherical impactor, a steel ball bearing with a diameter of 0.281 inch, a weight of 1.48 grams (0.00326 lb), and a mass of 0.00101 lb sec^2/ft. The target chamber area (see Figure 3) contained a laser velocimeter and Cranz-Schardine camera to record impact events. The camera records 20 frames on a 4" x 5" film with frame intervals of 100 microseconds. A typical Cranz-Schardine frame, as shown in Figure 4, shows the spherical impactor traveling left to right, clamped composite coupon, and reference object used for distance measurements. A typical frame sequence, as shown in Figure 5, shows the coupon and ball impactor before impact, during impact, coupon response, and ball impactor rebound. Impact velocities were grouped into three ranges: low, medium, and high ($\sim$200 ft/sec, $\sim$275 ft/sec, and $\sim$350 ft/sec, respectively) with variations in velocity due to the fit of the plastic sabot in the 50-caliber light gas gun and gas pressure.

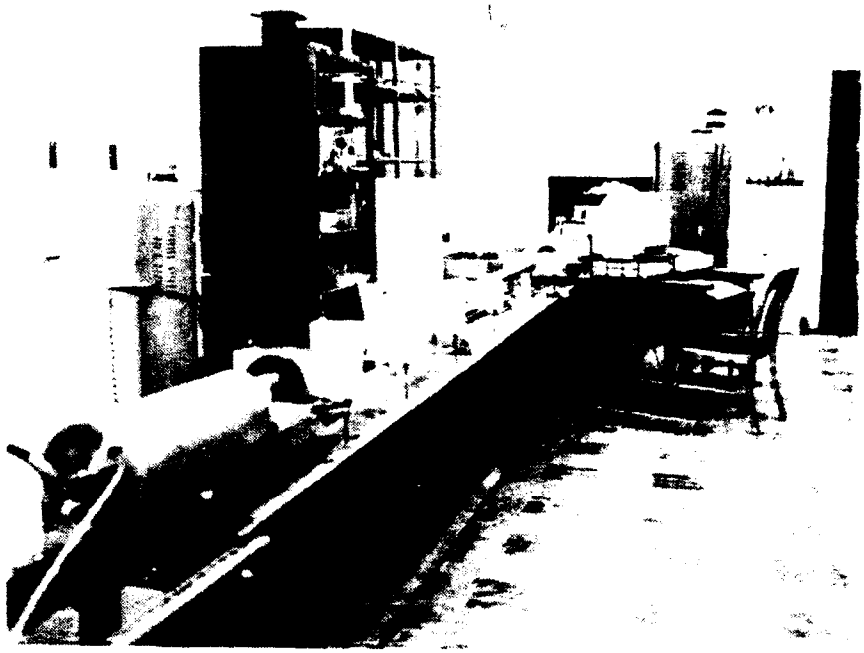

Figure 2. 50-caliber gas gun.

Figure 3. Target chamber area containing a laser velocimeter and Cranz-Schardine camera.

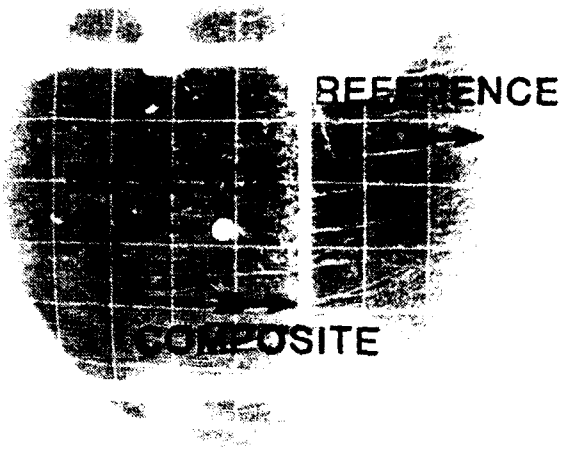

Figure 4. Typical Cranz-Schardine frame showing: (1) spherical impactor traveling left to right; (2) clamped composite coupon; and (3) reference object for distance measurements.

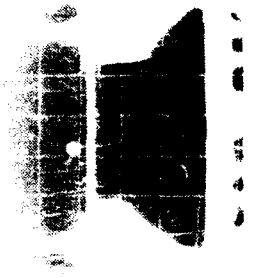

(a) Ball Impact

(b) Impact

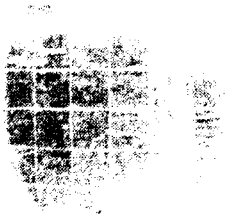

(c) Coupon Response

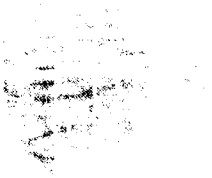

(d) Ball Impactor Rebound

Figure 5. Typical Cranz-Schardine sequence: (a) before impact; (b) impact; (c) coupon response, and (d) ball impactor rebound.

Resulting impact damage created front and rear surface delaminations and local fiber breakage at the point of impact. Front surface delamination is shown in Figures 6 through 8 for $[(0/90)_4]_s$, $[(+45/-45)_4]_s$, and $[(0/+45/-45/90)_2]_s$ laminate orientations, respectively. Back or rear surface delamination was not photographed or characterized; however, the delamination area was greater in extent in each case. Figure 9 shows the front surface delamination area as a function of laminate orientation at the medium velocity range. Delamination patterns can be seen that correspond to laminate orientations. The delamination areas of the front surface are given in Table 3, along with impact velocities and calculated input energy.

Table 3. Experimental parameters and resulting front surface delamination area

Laminate	Velocity* (ft/sec)	Input energy (ft-lb)	Delamination area (square inches)
$[(0/90)_4]_s$	206 L	1.541	0.152
	286 M	3.010	0.411
	333 H	3.396	0.628
$[(+45/-45)_4]_s$	199 L	1.248	0.152
	261 M	3.535	0.295
	380 H	3.634	0.541
$[(0/+45/-45/90)_2]_s$	221 L	1.651	0.396
	276 M	3.885	0.528
	333 H	4.705	1.214

NOTE: * Velocities are grouped into three ranges: L = low, M = medium, and H = high

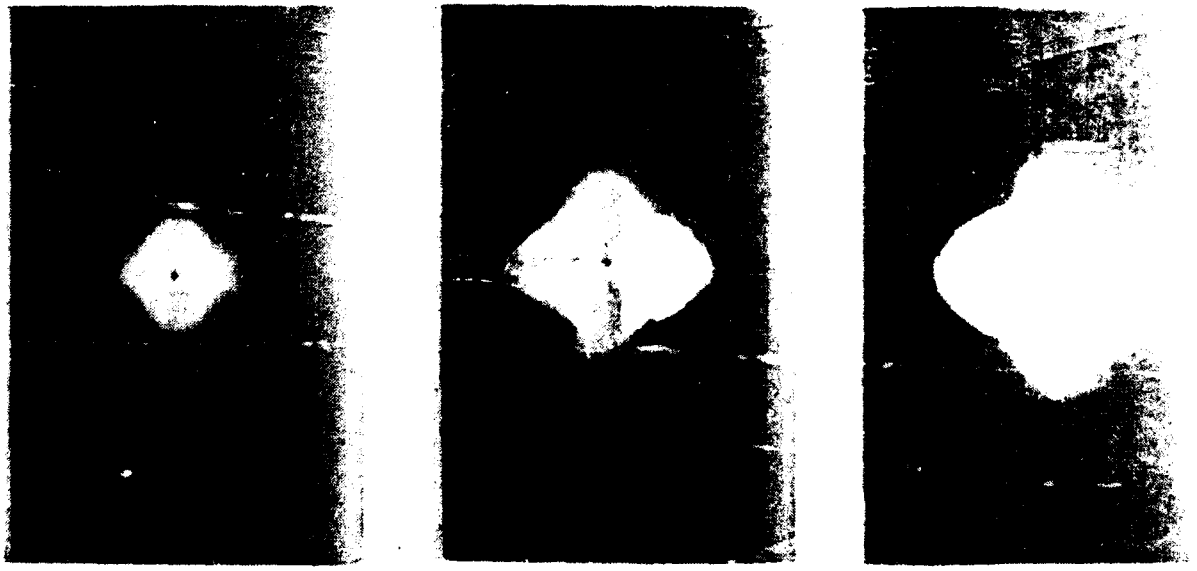

(a) (b) (c)

Figure 6. Front surface delamination area as a function of input energy for $[(0/90)_4]_s$ laminate: (a) input energy - 1.541 ft-lbf and delamination area - 0.152 sq. in.; (b) input energy - 3.010 ft-lbf and delamination area - 0.411 sq. in. and (c) input energy -.3.396 ft-lbf and delamination area - 0.628 sq. in.

(a) (b) (c)

Figure 7. Front surface delamination area as a function of input energy for $[(+45/-45)_4]_S$ laminate (a) input energy 1.248 ft-lbf and delamination area - 0.152 sq. in., (b) input energy - 3.535 ft-lbf and delamination area - 0.295 sq. in and (c) input energy - 3.634 ft-lbf and delamination area - 0.541 sq. in.

(a) (b) (c)

Figure 8. Front surface delamination area as a function of input energy for $[(0/+45/-45/90)_2]_S$ laminate (a) input energy - 1.651 ft-lbf and delamination area - 0.396 sq. in., (b) input energy - 3.885 ft-lbf and delamination area - 0.528 sq. in., and (c) input energy - 4.720 ft-lbf and delamination area - 1.215 sq. in

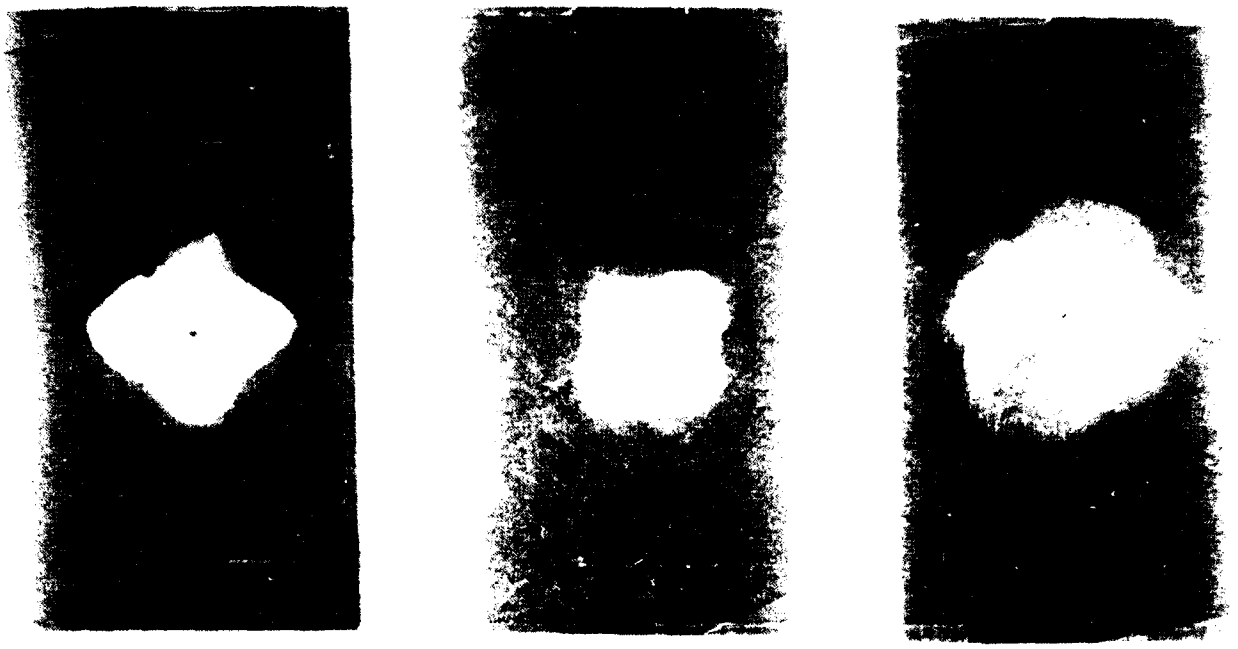

(a) $[(0/90)_4]_s$ (b) $[(+45/-45)_4]_s$ (c) $[0/+45/-45/90)_2]_s$

Figure 9. Front surface delamination area as a function of laminate orientation: (a) input energy - 3.010 ft-lbf; (b) input energy - 3.535 ft-lbf; and (c) input energy - 3.885 ft-lbf.

Impact damage coupons were prepared for moire by coating the coupon surfaces with a thin layer of epoxy to smooth the surface, applying a thin coat of white paint, and finally applying a 500-dot-per-inch moire film emulsion grating. These coupons were photographed during tensile loading in steps of 10% ultimate failure load determined from the streamline coupons and effective laminate properties given previously in Table 2, and, subsequently, optically processed [8]. The processing allowed u and v front surface displacement contours to be obtained independently and displacement sensitivity to be multiplied by a factor of two to obtain a resolution of 0.001 inch displacement per fringe. This optical processing arrangement is shown in Figure 10, and schematically in Figure 11. The arrangement consists of a helium neon laser, transform lenses and fourier filtering apertures, and 1000-lines-per-inch reference grating and recording camera. Resulting v-displacement moire fringe patterns or displacement contours for the three laminate orientations at various load levels are shown in Figures 12 to 19. The fringes run horizontally with a higher concentration in the damage area. The u-displacement contours not shown had only two or three fringes running in the vertical direction. This fringe density was not adequate for strain evaluation.

The displacement contours at the various load levels were examined visually in the optical processing system. Not all were photographed because at the lower load levels fringe patterns did not change, and at higher load levels coupons slipped in the loading grips or the moire grating was damaged in the loading process.

(a)

(b)

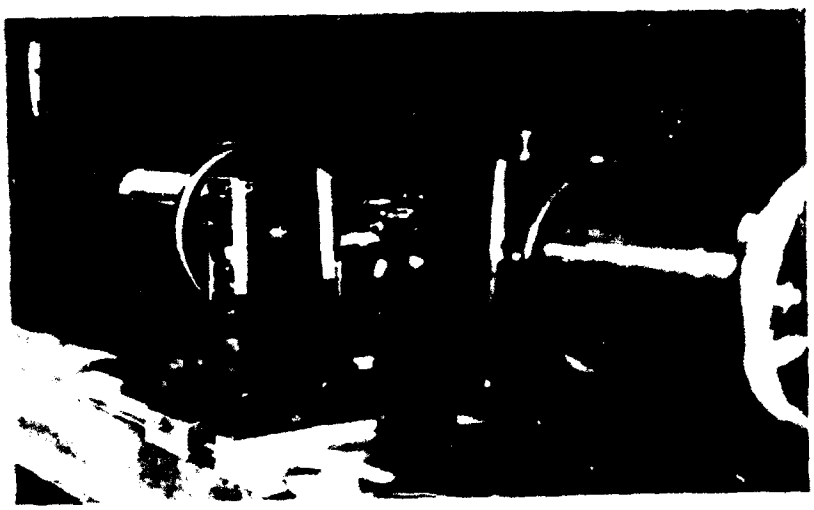

Figure 10 Optical processing arrangement: (a) optical rail showing recording camera at far end of rail, 1000-line-per-inch reference grating, and transform lenses and filtering apertures; and (b) enlarged view of transform lenses and filtering apertures

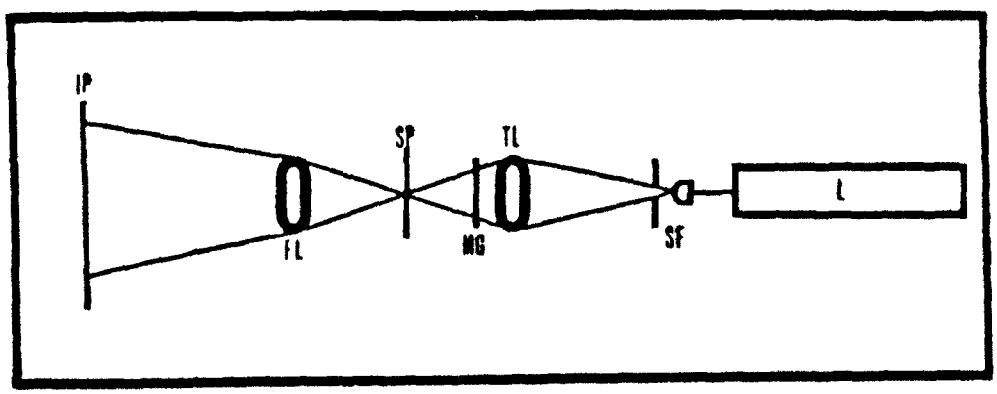

Figure 11 Schematic of optical processing arrangement: IP = image plane; FL = field lens; L = laser MG = moire grating; SF = spatial filter; SP = spectrum plane; and TL = transform lens.

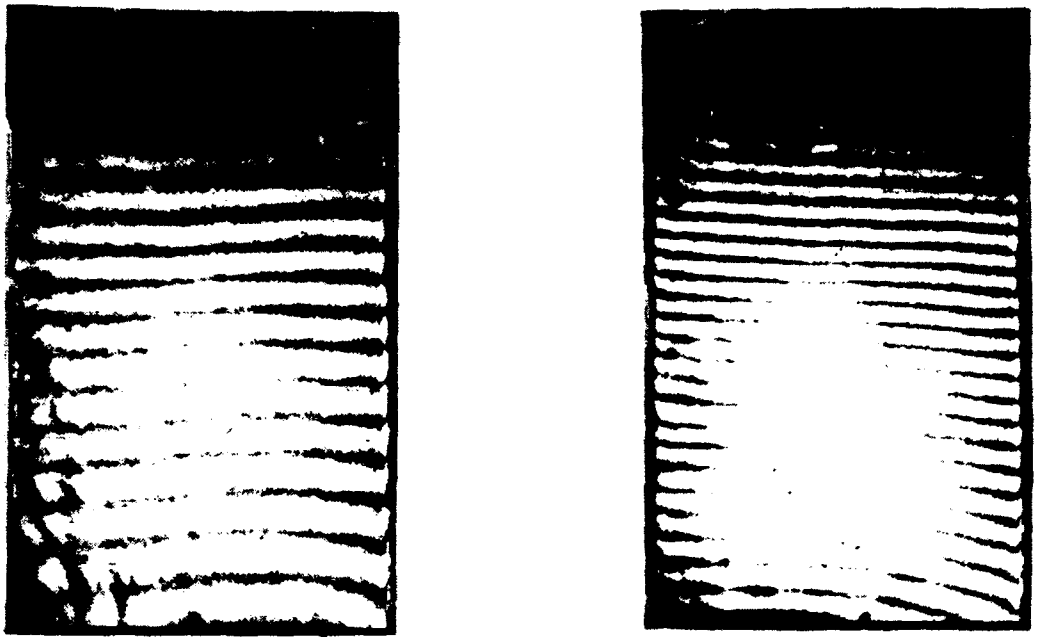

(a) 40% (b) 60%

Figure 12. Displacement contours for $[(0/90)_4]_s$ laminate and impact energy of 3.010 ft-lbf at: (a) 40% ultimate load level; and (b) 60% ultimate load level.

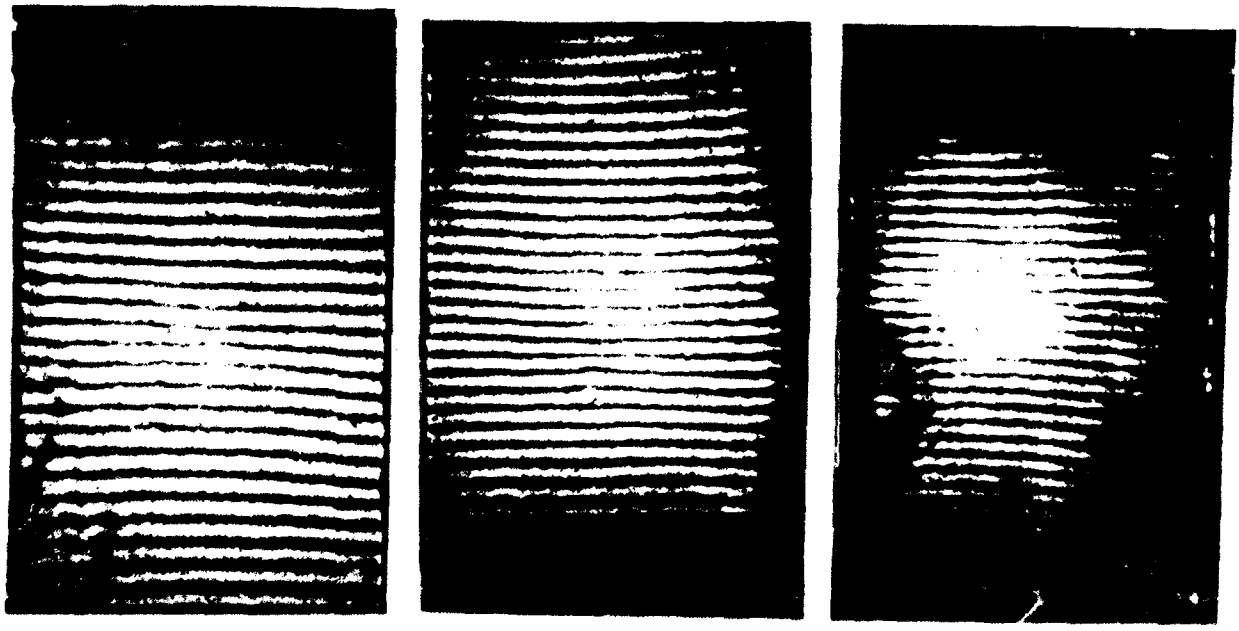

(a) 50% (b) 60% (c) 70%

Figure 13. Displacement contours for $[(0/90)_4]_s$ laminate and impact energy of 3.010 ft-lbf at: (a) 50% ultimate load level; (b) 60% ultimate load level; and (c) 70% ultimate load level.

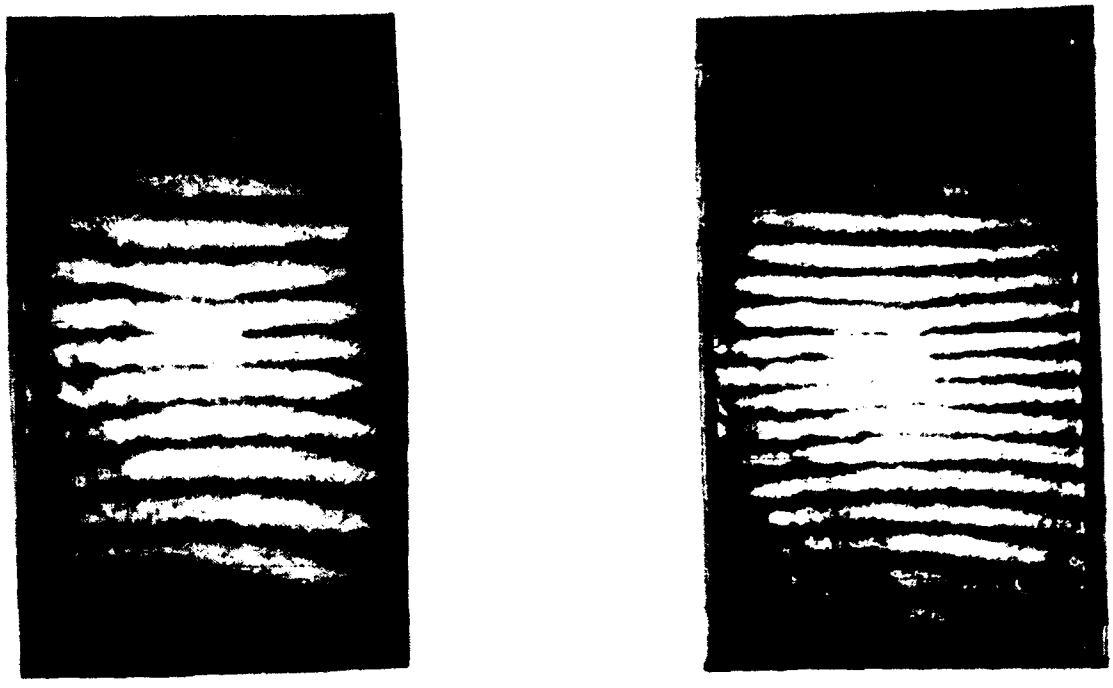

(a) 30%

(b) 40%

Figure 14. Displacement contours for $[(0/90)_4]_s$ laminate and impact energy of 3.396 ft-lbf at: (a) 30 ultimate load level; and (b) 40% ultimate load level.

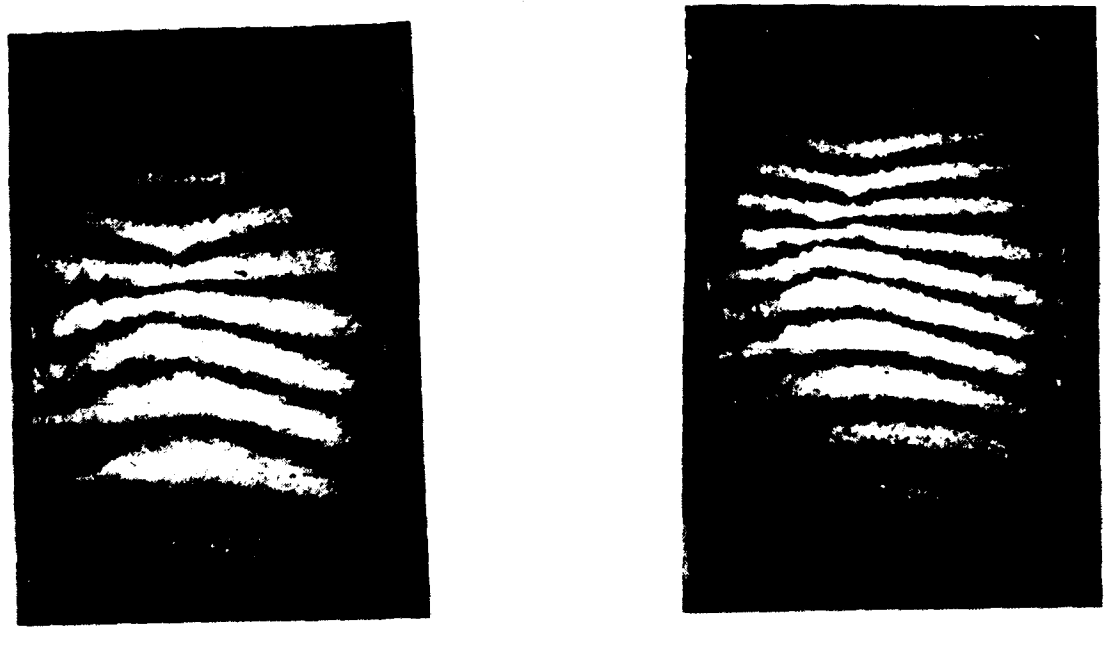

(a) 50%

(b) 60%

Figure 15. Displacement contours for $[(+45/-45)_4]_s$ laminate and impact energy of 1.248 ft-lbf at: (a) 50% ultimate load level; and (b) 60% ultimate load level.

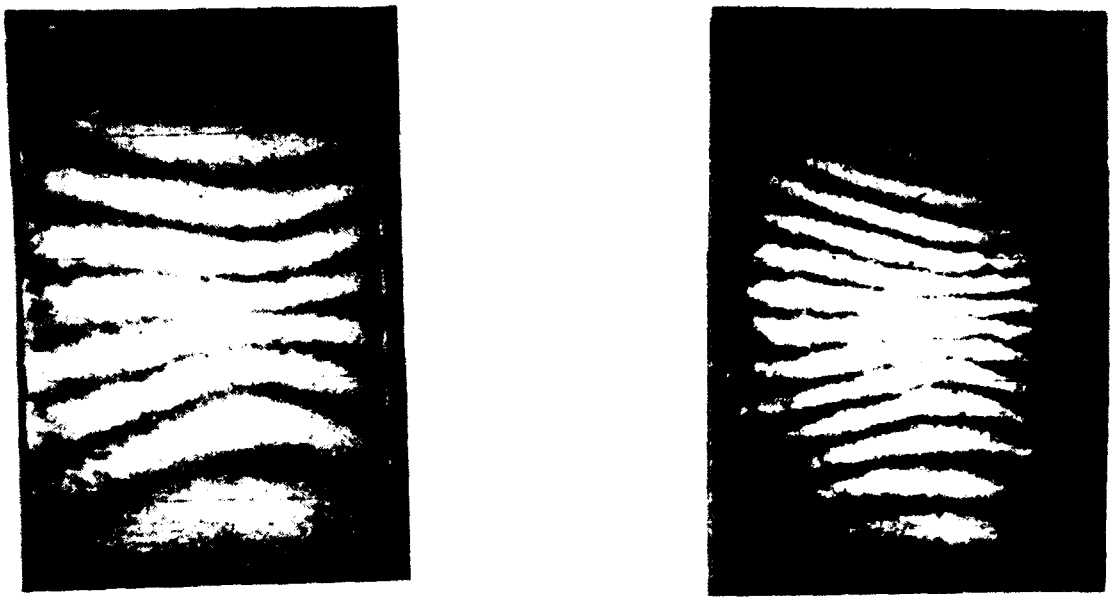

(a) 50% (b) 60%

Figure 16. Displacement contours for $[(+45/-45)_4]_s$ laminate and impact energy of 3.535 ft-lbf at: (a) 50% ultimate load level; and (b) 60% ultimate load level.

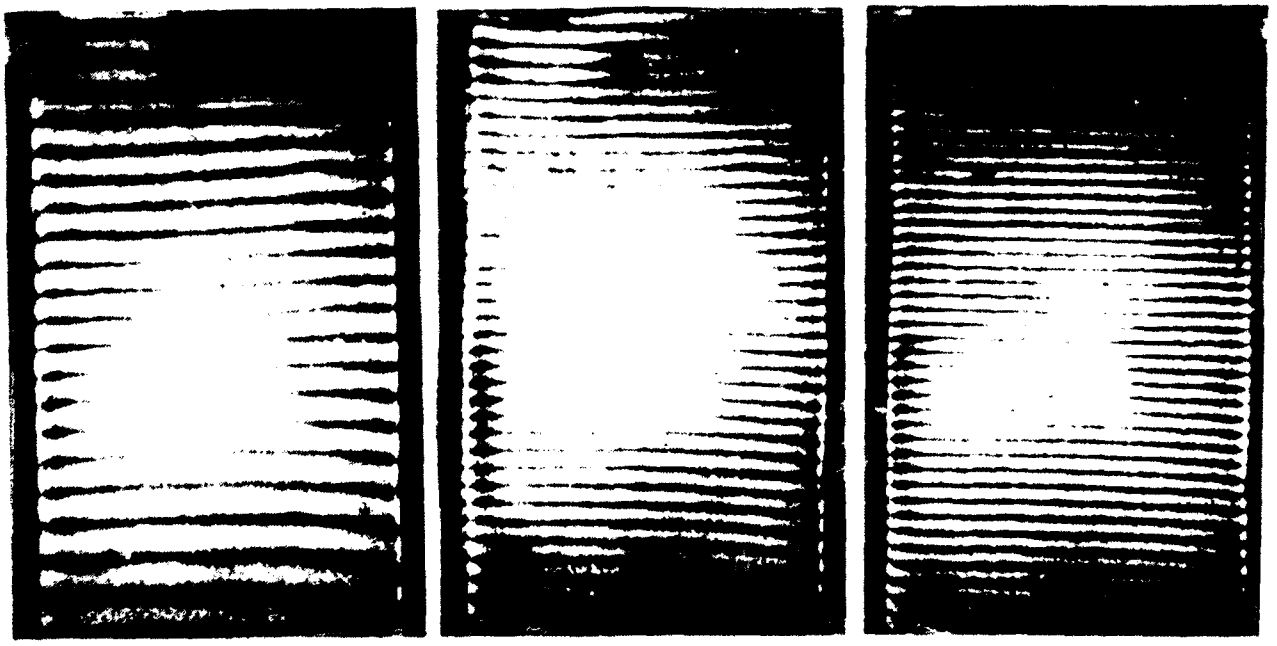

(a) 40% (b) 60% (c) 70%

Figure 17. Displacement contours for $[(0/+45/-45/90)_2]_s$ laminate and impact energy of 1.651 ft-lbf at: (a) 40% ultimate load level; (b) 60% ultimate load level; and (c) 70% ultimate load level.

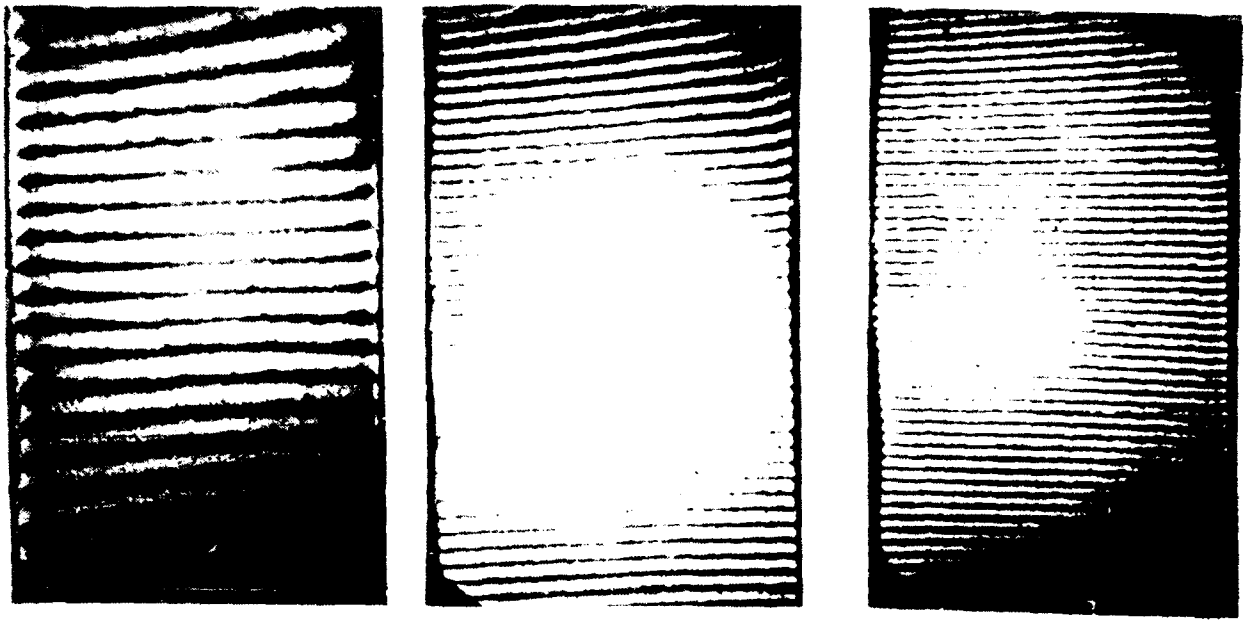

(a) 40% (b) 60% (c) 80%

Figure 18. Displacement contours for $[(0/+45/-45/90_2]_s$ laminate and impact energy of 3.885 ft-lbf at: (a) 40% ultimate load level; (b) 60% ultimate load level: and (c) 80% ultimate load level.

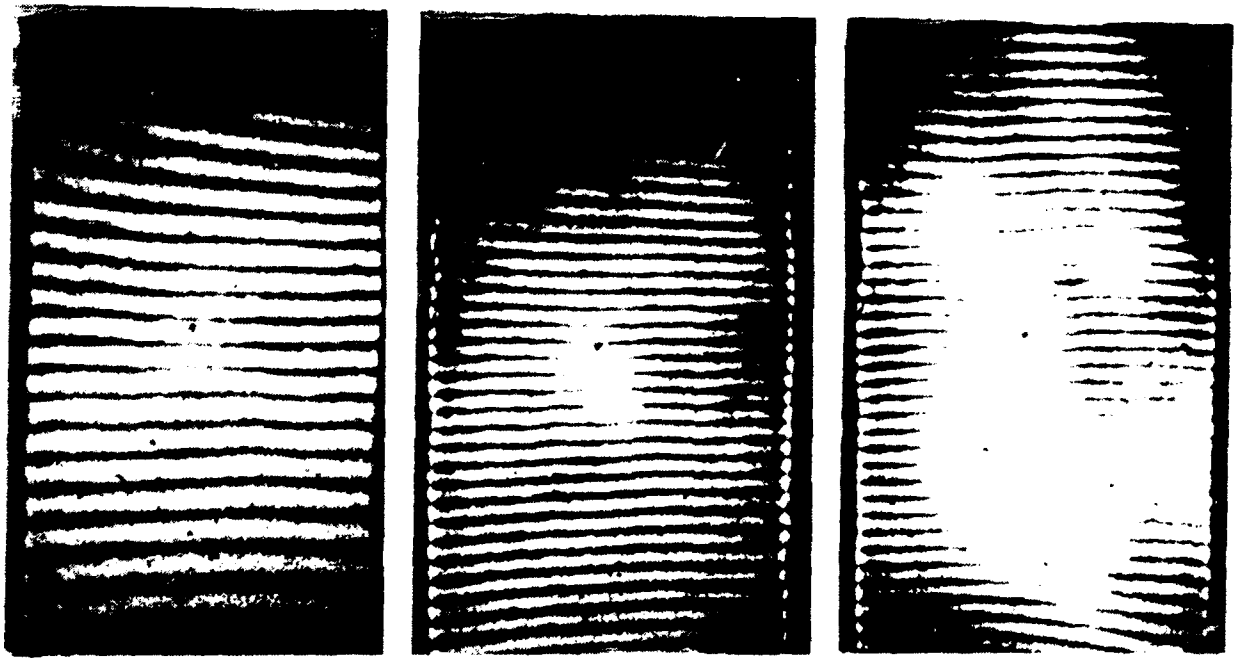

(a) 40% (b) 60% (c) 70%

Figure 19. Displacement contours of $[(0/+45/-45/90)_2]_s$ laminate and impact energy of 4.720 ft-lbf at: (a) 40% ultimate load level; (b) 60% ultimate load level; and (c) 70% ultimate load level.

Strains in the y-direction, $\varepsilon_y = \partial v/\partial y$, were obtained graphically by numbering the fringes, plotting fringe number versus fringe location, and then taking the slope of the plot at the point of highest concentration. Far field strains were calculated using Hooke's law, y-direction effective modulus from Table 2, coupon cross-sectional area, and the load at which the displacement contours were recorded. Strain concentrations were obtained by dividing strain at the damage location by the far field strain. Results are shown in Table 4.

Table 4. Experimental values of strain concentration

Laminate	Velocity	Strain Concentration at %				Ultimate Load	
		30	40	50	60	70	80
$[(0/90)_4]_s$	L	--	1.0	--	1.0	--	*
	M	--	--	1.1	1.41	1.55	*
	H	1.89	2.46	*	*	*	*
$[(+45/-45)_4]_s$	L	--	--	2.00	2.07	*	*
	M	--	--	1.73	2.10	*	*
	H	*	*	*	*	*	*
$[(0/+45/-45/90)_2]_s$	L	--	1.0	--	1.0	1.0	*
	M	--	1.0	--	1.0	*	1.0
	H	--	1.0	--	1.59	1.69	*

NOTE: -- Denotes no measurements were made; * Denotes coupon slipped in grips or grating failed

Conclusions

This paper demonstrates that moire techniques can be used to obtain strain concentration factors of low velocity impact damaged glass/epoxy composite material. The displacement sensitivity, however, was a limiting factor that did not allow for strain concentration assessment of the coupons damaged at the lower impact energies, nor is interlamina decoupling noticeable at delamination boundaries in the fringe contours. Even with this limiting factor, some observations are possible. Delamination area as a function of velocity or input energy increases as expected and exhibit delamination patterns corresponding to the laminate orientations. The $[(0/+45/-45/90)_2]_s$ laminate exhibited the largest delamination areas but did not have the largest strain concentration factor for similar input energies. This shows that the $[(0/+45/-45/90)_2]_s$ laminate transferred the impact energy into creating larger delamination areas and less local fiber damage; thus, this laminate is more structurally resilient in tension to damage from low velocity impacts.

References

1. THEOCARIS, P.S. *Moire Fringes in Strain Analysis*. Pergamon Press, 1969.
2. DURELLI, A. J., and PARKS, V. J. *Moire Analysis of Strain*. Prentice-Hall, Inc., 1970.
3. CHIANG, F. P *Moire Methods of Strain Analysis*. Manual on Experimental Stress Analysis, Society for Experimental Stress Analysis, ch. 5, 1978.
4. PARKS, V. J. *Geometric Moire*. Society for Experimental Mechanics (SEM) Handbook on Experimental Stress Analysis, A. Kobayashi, ed., ch. 6, 1984.
5. OPLINGER, D.W. *On the Streamline Specimen for Tension Testing of Composite Materials*. American Society for Testing and Materials, 1985.
6. JONES, R. M. *Mechanics of Composite Materials*. Hemisphere Publishing Corporation, New York, NY, 1975.
7. HALPIN, J. C. *Primer on Composite Material: Analysis*. Technomic Publishing Company, Inc., Lancaster, PA, 1984.
8. CHIANG, F.P., PARKER, B.S., OPLINGER, D.W., and SLEPETZ, J.M. *Theory and Technology of Moire Methods*. U.S. Army Materials and Mechanics Research Center (AMMRC), Watertown, MA. Report SP 80-4, April 1980.

DISTRIBUTION LIST

No. of Copies	To
1	Office of the Under Secretary of Defense fo: Research and Engineering, The Pentagon, Washington, DC 20301
	Director, U.S. Army Research Laboratory, 2800 Powder Mill Road, Adelphi, MD 20783-1197
1	ATTN: AMSRL-OP-CI-A
	Commander, Defense Technical Information Center, Cameron Station, Building 5, 5010 Duke Street, Alexandria, VA 22304-6145
1	ATTN: DTIC-FDAC
1	MIA/CINDAS, Purdue University, 2595 Yeager Road, West Lafayette, IN 47905
	Commander, Army Research Office, P.O. Box 12211, Research Triangle Park, NC 27709-2211
1	ATTN: Information Processing Office
	Commander, U.S. Army Materiel Command, 5001 Eisenhower Avenue, Alexandria, VA 22333
1	ATTN: AMCSCI
	Commander, U.S. Army Materiel Systems Analysis Activity, Aberdeen Proving Ground, MD 21005
1	ATTN: AMXSY-MP, H. Cohen
	Commander, U.S. Army Missile Command, Redstone Arsenal, AL 35809
1	ATTN: AMSMI-RD-CS-R/Doc
	Commander, U.S. Army Armament, Munitions and Chemical Command, Dover, NJ 07801
2	ATTN: Technical Library
	Commander, U.S. Army Natick Research, Development and Engineering Center, Natick, MA 01760-5010
1	ATTN: Technical Library
	Commander, U.S. Army Satellite Communications Agency, Fort Monmouth, NJ 07703
1	ATTN: Technical Document Center
	Commander, U.S. Army Tank-Automotive Command, Warren, MI 48397-5000
1	ATTN: AMSTA-ZSK
1	AMSTA-TSL, Technical Library
	Commander, White Sands Missile Range, NM 88002
1	ATTN: STEWS-WS-VT
	President, Airborne, Electronics and Special Warfare Board, Fort Bragg, NC 28307
1	ATTN: Library
	Director, U.S. Army Ballistic Research Laboratory, Aberdeen Proving Ground, MD 21005
1	ATTN: SLCBR-TSB-S (STINFO)
	Commander, Dugway Proving Ground, UT 84022
1	ATTN: Technical Library, Technical Information Division
	Commander, Harry Diamond Laboratories, 2800 Powder Mill Road, Adelphi, MD 20783
1	ATTN: Technical Information Office
	Director, Benet Weapons Laboratory, LCWSL, USA AMCCOM, Watervliet, NY 12189
1	ATTN: AMSMC-LCB-TL
1	AMSMC-LCB-R
1	AMSMC-LCB-RM
1	AMSMC-LCB-RP
	Commander, U.S. Army Foreign Science and Technology Center, 220 7th Street, N.E., Charlottesville, VA 22901-5396
3	ATTN: AIFRTC, Applied Technologies Branch, Gerald Schlesinger
	Commander, U.S. Army Aeromedical Research Unit, P.O. Box 577, Fort Rucker, AL 36360
1	ATTN: Technical Library

No. of Copies	To
	Commander, U.S. Army Aviation Systems Command, Aviation Research and Technology Activity, Aviation Applied Technology Directorate, Fort Eustis, VA 23604-5577
1	ATTN: SAVDL-E-MOS
	U.S. Army Aviation Training Library, Fort Rucker, AL 36360
1	ATTN: Building 5906-5907
	Commander, U.S. Army Agency for Aviation Safety, Fort Rucker, AL 36362
1	ATTN: Technical Library
	Commander, Clarke Engineer School Library, 3202 Nebraska Ave., N, Ft. Leonard Wood, MO 65473-5000
1	ATTN: Library
	Commander, U.S. Army Engineer Waterways Experiment Station, P.O. Box 631, Vicksburg, MS 39180
1	ATTN: Research Center Library
	Commandant, U.S. Army Quartermaster School, Fort Lee, VA 23801
1	ATTN: Quartermaster School Library
	Naval Research Laboratory, Washington, DC 20375
1	ATTN: Code 5830
2	Dr. G. R. Yoder - Code 6384
	Chief of Naval Research, Arlington, VA 22217
1	ATTN: Code 471
	Commander, U.S. Air Force Wright Research & Development Center, Wright-Patterson Air Force Base, OH 45433-6523
1	ATTN: WRDC/MLLP, M. Forney, Jr.
1	WRDC/MLBC, Mr. Stanley Schulman
	NASA - Marshall Space Flight Center, MSFC, AL 35812
1	ATTN: Mr. Paul Schuerer/EH01
	U.S. Department of Commerce, National Institute of Standards and Technology, Gaitherburg, MD 20899
1	ATTN: Stephen M. Hsu, Chief, Ceramics Division, Institute for Materials Science and Engineering
1	Committee on Marine Structures, Marine Board, National Research Council, 2101 Constitution Avenue, N.W., Washington, DC 20418
1	Materials Sciences Corporation, Suite 250, 500 Office Center Drive, Fort Washington, PA 19034
1	Charles Stark Draper Laboratory, 555 Technology Square, Cambridge, MA 02139
	Wyman-Gordon Company, Worcester, MA 01601
1	ATTN: Technical Library
	General Dynamics, Convair Aerospace Division P.O. Box 748, Forth Worth, TX 76101
1	ATTN: Mfg. Engineering Technical Library
	Plastics Technical Evaluation Center, PLASTEC, ARDEC Bldg. 355N, Picatinny Arsenal, NJ 07806-5000
1	ATTN: Harry Pebly
1	Department of the Army, Aerostructures Directorate, MS-266, U.S. Army Aviation R&T Activity - AVSCOM, Langley Research Center, Hampton, VA 23665-5225
1	NASA - Langley Research Center, Hampton, VA 23665-5225
1	U.S. Army Propulsion Directorate, NASA Lewis Research Center, 2100 Brookpark Road, Cleveland, OH 44135-3191
1	NASA - Lewis Research Center, 2100 Brookpark Road, Cleveland, OH 44135-3191
	Director, Defense Intelligence Agency, Washington, DC 20340-6053
1	ATTN: ODT-5A (Mr. Frank Jaeger)
	Director, U.S. Army Research Laboratory, Watertown, MA 02172-0001
2	ATTN: AMSRL-OP-CI-D, Technical Library
10	Authors